

Aircraft system identification using simultaneous quantized harmonic input signals

P. LICHOTA*

Institute of Aeronautics and Applied Mechanics, ul. Nowowiejska 24, 00-665 Warsaw, Poland

Abstract. In this paper, quantized multisine inputs for a maneuver with simultaneous elevator, aileron and rudder deflections are presented. The inputs were designed for 9 quantization levels. A nonlinear aircraft model was excited with the designed inputs and its stability and control derivatives were identified. Time domain output error method with maximum likelihood principle and a linear aircraft model were used to perform parameter estimation. Visual match and relative standard deviations of the estimates were used to validate the results for each quantization level for clean signals and signals with measurement noise present in the data. The noise was included into both output and input signals. It was shown that it is possible to obtain accurate results when simultaneous flight controls deflections are quantized and noise is present in the data.

Key words: system identification, input design, flight dynamics.

1. Introduction

Full flight simulators are large-scale devices that imitate cockpit design and the behavior of a particular aircraft. They can be used to perform numerous tasks e.g. pilot training, military operation planning, aircraft accident investigation or object redesign. According to regulations, those devices contain a dynamical model of the aircraft that must be obtained from the flight test campaign [1, 2]. This makes full flight simulator development very costly, because the data cannot be gathered during scheduled flights (specific experiments are required) and the dedicated flight tests last multiple flight hours [3]. Despite the high cost in aeronautics, the system identification is widely used for airplanes [4, 5], rotorcrafts [6, 7], projectiles [8, 9] or pilot modelling [10, 11] as it delivers very accurate mathematical models of these objects.

The flight campaign time can be shortened by performing parameter identification in near-real time e.g. by using method described in [4]. Another approach is to design a flight plan in which multiple experiments are performed at the same time i.e. various flight controls are deflected simultaneously. It was already shown that this can be done without degrading the accuracy of the obtained model when multi-step [12, 13] or multisine experiments are used [14]. When multi-step signals are selected for a maneuver with simultaneous flight controls deflections their application must be preceded by a time consuming optimization. Therefore, those inputs cannot be used for redesigning experiments during the flight campaign (e.g. for flight envelope expansion).

Multisine inputs do not have those limitations and were already widely investigated. When multisine signals are used

their frequency resolution must be properly selected to excite all significant modes of the dynamical object. The aspect of multisine frequency resolution was discussed in [15]. The number of harmonics (which is a related feature when bandwidth is fixed), was shown in [16] for pilot modelling and path tracking. Manoeuvres with combined multisine and pilot inputs for aircraft system identification were used in [17]. Skipping selected harmonics of the multisine signals can be used to reduce nonlinear distortions. In [18] a system identification hardware for designing odd-multisines was presented. No interharmonic distortion multisines were used in [19] for the best linear approximation of a system with friction. The improved method for quasi-logarithmic multisines design was shown in [20]. Multisine energy content is defined also by power stored at certain frequencies. Thus, it is possible to optimize harmonic components amplitudes. In [21] D-optimality criterion and genetic algorithm were used to design multisines power spectrum. In [22] a technique for energy content design based on D-optimality and frequency responses was presented. Maximizing multisines efficiency is possible through phase angles selections. Direct numerical formulas that outperform the Schroeder approach for phase angles selection [23] were shown in [24]. An optimization algorithm for synthesizing multisines with arbitrary power spectrum was shown in [25]. Complexity and the cost of the measurement and processing equipment for multisine signals can be lowered by using algorithms that enable output under-sampling shown in [26]. In [27] the spectral estimation approach and using those signals in noise presence was analyzed. This was also done for simultaneous multisine inputs in [28], where additionally the time domain approach was used for validation.

As multisine signals consist of summed harmonic sinusoids, their application may be limited when it is not possible to faithfully reproduce their shape. Thus, it was decided to investigate if it is possible to use quantized multisines (allowed to

*e-mail: piotr.lichota@pw.edu.pl

Manuscript submitted 2020-06-16, revised 2020-09-19, initially accepted for publication 2020-09-21, published in December 2020

accept only a certain number of states) for aircraft system identification.

The multi-step signals have continuous power spectrum, whereas the multisines energy is discrete. This makes the identification with multisine inputs less robust than when step inputs are used due to spectral leakage and noise presence. The quantized multisine input can be viewed as a multi-step input that was designed in a novel way. It has a continuous power spectrum that increases the input robustness and is obtained in almost real time. The optimization time is approximately 3 minutes whereas for the D-optimal design providing comparable accuracy it takes approximately 2 hours when the design process shown in [12] is used. Thus, the quantized multisine signals would be useful, e.g. in online experiment design. Moreover, due to their ease in application they can also be used when it is not possible to generate input signals by flight management system or autopilot, e.g. in pilot model system identification tasks. Thus, quantized multisine inputs allow to combine best features of multi-step and multisines signals – ease of application and robustness of the multi-step signals with the multisines possibility of simultaneous flight controls deflections without long-lasting input design process (required when multi-step signals are optimized [12]). Analysis of the quantized multisines used for aircraft system identification is the main novelty of this paper.

The paper is organized as follows. In Section 2 multisine inputs and their quantization is described. In Section 3 model under test and its linear representation that is used for system identification are presented. The parameter estimation process is described in Section 4. The outcomes obtained for various numbers of quantization levels for clean data and data with measurement noise are presented in Section 5. To validate the outcomes relative standard deviations of the estimates and data not used in the system identification were used. Moreover, to verify the results, identification was also performed from frequency responses. Additionally, the measurement noise effect was considered for both – measurement noise in the outputs and in the inputs. The paper finishes with a short summary of conclusions.

The novelty of the paper comes from the consideration of using quantized multisines for aircraft system identification. It was investigated not only if it is possible to obtain accurate results when simultaneous flight controls are excited with quantized multisines signals, but at what quantization level the estimates would still be of high accuracy. This was assessed for an ideal case with no noise present, for typical aircraft system identification case, i.e. when measurement noise is present in the outputs and for a case when the noise is observed in the inputs (what represents unmodelled effects in input application). Results obtained with the time-domain output error method for the noise-free case were verified through identification from frequency responses. A simulation model of F-16 aircraft was used in the study as it faithfully represents the object dynamic vehicle responses. This allowed to avoid large costs of the study, what would happen in case of performing a dedicated flight campaign.

This article focuses on the quantized multisine inputs application for aircraft system identification. This study was approached as follows: design the inputs and identify aircraft parameters that allow to assess the pros and cons of the quantized multisines inputs when referred to other excitations. The identification method description is shown to give context to the reader and allow for results comparison when applying the approach.

2. Multisines

A multisine is a harmonic sum of sinusoids. If each flight control has a unique set of harmonics assigned, then the signal is mutually orthogonal in time and frequency domain. Thus, it is possible to deflect flight controls simultaneously without lowering information content in the output signals. In this study the SIDPAC package [14] was used to design those inputs.

Each flight control deflection was given as:

$$\delta_j = \delta_{j0} + \sum_{k \in M_j} A_k \sin(2\pi f_k t + \phi_k), \quad (1)$$

where δ_{j0} is the flight control deflection at trim point, k is the harmonic number from the M_j set assigned to a specific flight control, j is the flight control index, whilst A_k , f_k and ϕ_k are k -th harmonic amplitude, its frequency and phase shift.

The frequency resolution results from the excitation time T , i.e. $f_0 = 1/T$. To reduce costs and complexity of the measurement equipment used in aircraft system identification under-sampling can be used. Unfortunately, when multisine signals are used this increases the complexity of proper determination of the original signal. To prevent interference between excited frequencies (and thus lowered information in the data) the frequency spacing must be linear and double the frequency resolution [29]. Thus, the first harmonic is skipped. The harmonics are evenly spaced within the frequency range of interest $\langle f_{\min}, f_{\max} \rangle$, where $f_{\min} \leq 2f_0$.

If the same emphasis is put on all frequencies the amplitudes A_j are:

$$A_k = A_{j_{\max}} \sqrt{1/n_j}, \quad (2)$$

where $A_{j_{\max}}$ is the expected maximum amplitude increment for a specific flight control and n_j is the number of harmonics in the M_j set.

In order to ensure maximum energy of the input (represented by the input RMS) with minimum excitation range for each flight control, the Relative Peak Factor RPF is minimized

$$RPF(\delta_j) = \frac{\max(\delta_j) - \min(\delta_j)}{2\sqrt{2}rms(\delta_j)} \quad (3)$$

to determine phase shifts ϕ_k . After the optimization, it is also required to shift the excitations with respect to time, as they need to start and end with trim value.

In this research the excitation time was set to $T = 20$ s and the upper frequency bound was resulting from the aircraft rigid body dynamics $f_{\max} = 2$ Hz. The harmonic frequencies were

assigned alternately to elevator (δ_E), ailerons (δ_A) and rudder (δ_R). The expected maximum amplitude increment $A_{j_{max}}$ was set to 1 deg for each flight control. The input trim values δ_{j_0} were 0 deg for ailerons and rudder and -3.68 deg for elevator as it was required to be in straight symmetric steady flight before performing the excitation. Moreover, two 5 s lasting flight data segments (one before and one after the excitation) were included in the registered signals to allow for static terms estimation.

Designed input harmonic components are presented in Table 1 and the signals are shown in Fig. 1 (blue line). The *RPF*

Table 1
Multisine input components

Elevator		Ailerons		Rudder	
f_k , Hz	ϕ_k , rad	f_k , Hz	ϕ_k , rad	f_k , Hz	ϕ_k , rad
0.10	2.3515	0.15	-2.7835	0.20	0.7438
0.25	-0.1658	0.30	-1.4683	0.35	-2.2255
0.40	-2.7168	0.45	-0.6368	0.50	1.1458
0.55	-1.1792	0.60	-1.3347	0.65	1.8536
0.70	-2.1643	0.75	1.3458	0.80	0.4552
0.85	2.2099	0.90	-2.8503	0.95	-1.9192
1.00	0.5996	1.05	-1.3418	1.10	2.3372
1.15	1.1178	1.20	-2.6574	1.25	2.3409
1.30	2.0734	1.35	1.9800	1.40	2.7837
1.45	1.8409	1.50	-1.0806	1.55	2.1700
1.60	-0.5518	1.65	0.6659	1.70	-0.9612
1.75	0.7950	1.80	-1.1664	1.85	0.2534
1.90	2.3004	1.95	-1.6331	2.00	1.0095

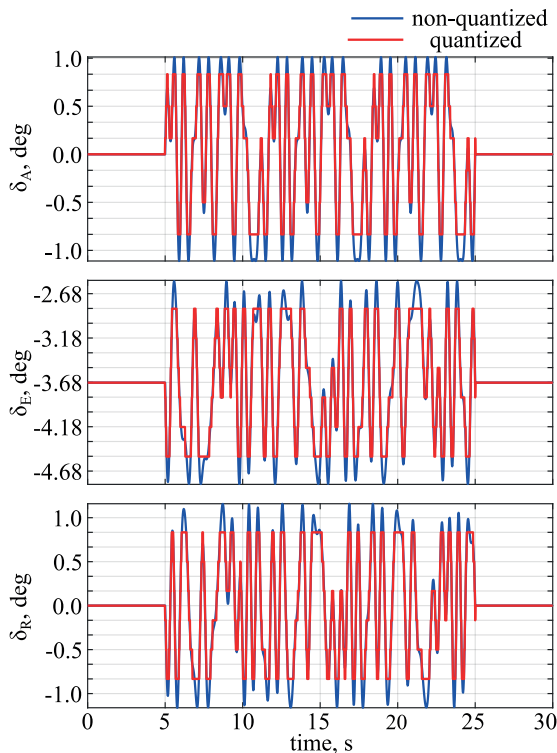


Fig. 1. Input signals

was 1.1453, 1.0621 and 1.1606 for elevator, ailerons and rudder respectively.

In this research, designed multisine excitations were quantized i.e. allowed to accept only certain values. The uniform mid-rise quantization was used for that purpose. The boundaries for the quantized signals were $\pm(A_{j_{max}} - A_{j_{max}}/m)$, where m is the number of quantization levels. The values that can be accepted by the signal were evenly spaced within those boundaries. Before and after the excitation the inputs were held at their trimmed values.

The multisine inputs were quantized for 16, 14, 12, 10, 8, 6, 4 and 2 levels. The odd quantization levels were not used as excitation did not hold zero value.

The quantized input with 6 possible states is presented in Fig. 1 (red line). From the plot it can be seen that in general the quantized input matches well the non-quantized one. Due to the quantized signals boundaries they cannot accept maximum values of the multisine signals. Moreover, the quantized inputs have problems with recapturing selected harmonics (e.g. at the thirteenth second for elevator deflection).

This can be also observed when looking at the power spectrum of the inputs in Fig. 2, where the non-quantized signal is denoted as ∞ . It can be seen that when the quantization was performed for 6, 4 and 2 levels, the power (representing possibility to obtain information at specified frequency) drops, which can result in less accurate estimates of the model parameters.

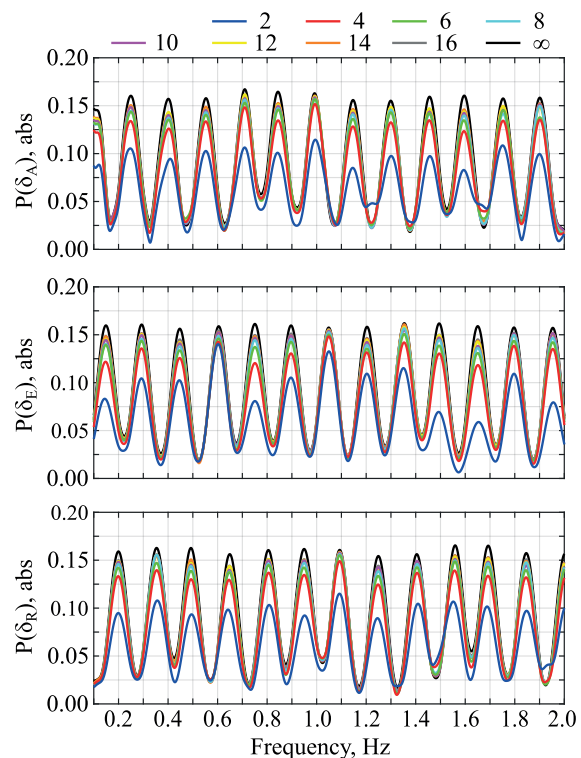


Fig. 2. Input power spectrum

If the multisine components had been represented as pulse signals and their phase angles were optimized then it still would be possible to deflect flight controls simultaneously. However this would mean that the signals are quantized at $2n_j$ levels,

where n_j is the number of harmonics in the M_j set. Limiting quantization levels by including additional constraints would increase the computational time. As the motivation was to combine features of the multi-step and multisine signals (ease in application and robustness with simultaneous deflections and fast design) this was not considered as a suitable approach to achieve present investigations aim.

3. Model

In order to assess the quality of quantized inputs a simulation model was used to represent a real aircraft. This approach is widely used in flight dynamics tasks in order to limit flight campaign costs when new developments or modifications are to be tested [30–32].

3.1. Nonlinear model. Inputs described in Section 2 were used to excite a nonlinear F-16 aircraft model.

The equations of motion were derived in body axes coordinate system $Oxyz$, origin of which was located at the aircraft centre of gravity. The coordinate system is presented in Fig. 3. The Ox axis lays in the symmetry plane and is parallel to wing mean aerodynamic chord. The Oy axis is directed towards the right wing and the Oz axis complements the right-handed set.

In Fig. 3, Earth fixed frame $O_1x_1y_1z_1$ and inertial system $Ox_gy_gz_g$ are presented as well. The inertial coordinate system is moving with the aircraft and is parallel to Earth-fixed frame. Tait-Bryan angles (bank angle ϕ , pitch angle θ , yaw angle ψ) describe orientation of the body axes reference frame with respect to gravitational system. The aircraft linear velocity \mathbf{V} components (u – longitudinal velocity, v – side velocity, w – vertical velocity) and angular velocity $\mathbf{\Omega}$ components (p – roll rate, q – pitch rate, r – yaw rate) are shown in Fig. 3 as well.

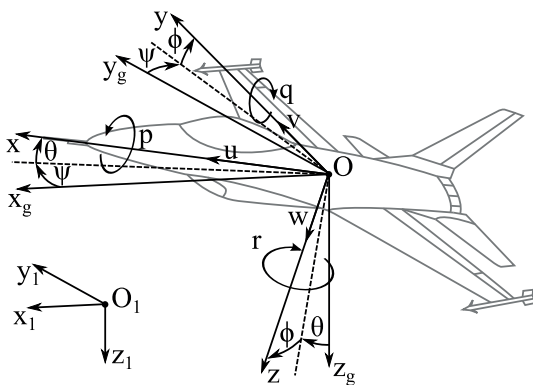


Fig. 3. Coordinate systems

Equations of motion were obtained from Newton second law of motion. Momentum $\mathbf{\Pi}$ and angular momentum \mathbf{K}_O change theorems in the rotating frame were as follows:

$$\begin{aligned} \dot{\mathbf{\Pi}} + \mathbf{\Omega} \times \mathbf{\Pi} &= \mathbf{F}, \\ \dot{\mathbf{K}}_O + \mathbf{\Omega} \times \mathbf{K}_O &= \mathbf{M}_O, \end{aligned} \quad (4)$$

where \mathbf{F} and \mathbf{M}_O stand for external force and moment, that depend on aerodynamics, thrust and gravitation. The dot symbol denotes time derivative.

For rigid body the momentum and angular momentum are given as:

$$\begin{aligned} \mathbf{\Pi} &= m\mathbf{V}_O, \\ \mathbf{K}_O &= \mathbf{I}\mathbf{\Omega}, \end{aligned} \quad (5)$$

where \mathbf{I} is the inertia matrix. Due to vertical symmetry plane (in terms of geometry and mass) inertia product $I_{xy} = 0$ and $I_{yz} = 0$.

This led to the following equations of motion:

$$\begin{aligned} \bar{q}SC_X + T - mg \sin \theta &= m(\dot{u} + qw - rv), \\ \bar{q}SC_Y + mg \sin \phi \cos \theta &= m(\dot{v} + ru - pw), \\ \bar{q}SC_Z + mg \cos \phi \sin \theta &= m(\dot{w} + pv - qu), \\ C_l \bar{q}Sb &= I_{xx}\dot{p} - I_{xz}\dot{r} + (I_{zz} - I_{yy})qr - I_{xz}pq, \\ C_m \bar{q}S\bar{c} - rH_T &= I_{yy}\dot{q} + (I_{xx} - I_{zz})pr + I_{xz}(p^2 - r^2), \\ C_n \bar{q}Sb + qH_T &= I_{zz}\dot{r} - I_{xz}\dot{p} + (I_{yy} - I_{xx})pq + I_{xz}qr, \end{aligned} \quad (6)$$

where \bar{q} is the dynamic pressure, S is the wing area, \bar{c} is the mean aerodynamic chord and b is the wingspan. C_X , C_Y and C_Z are longitudinal, side and vertical aerodynamic force nondimensional coefficients, and C_l , C_m and C_n are roll, pitch and yaw aerodynamic moment coefficients, respectively:

$$\begin{aligned} C_X &= C_{X_0} + C_{X_\alpha} \alpha + C_{X_q} q^* + C_{X_{\delta_E}} \delta_E, \\ C_Y &= C_{Y_0} + C_{Y_\beta} \beta + C_{Y_p} p^* + C_{Y_r} r^* + C_{Y_{\delta_A}} \delta_A + C_{Y_{\delta_R}} \delta_R, \\ C_Z &= C_{Z_0} + C_{Z_\alpha} \alpha + C_{Z_\beta} \beta + C_{Z_q} q^* + C_{Z_{\delta_E}} \delta_E, \\ C_l &= C_{l_0} + C_{l_\beta} \beta + C_{l_p} p^* + C_{l_r} r^* + C_{l_{\delta_A}} \delta_A + C_{l_{\delta_R}} \delta_R, \\ C_m &= C_{m_0} + C_{m_\alpha} \alpha + C_{m_q} q^* + C_{m_{\delta_E}} \delta_E, \\ C_n &= C_{n_0} + C_{n_\beta} \beta + C_{n_p} p^* + C_{n_r} r^* + C_{n_{\delta_A}} \delta_A + C_{n_{\delta_R}} \delta_R. \end{aligned} \quad (7)$$

The aerodynamic force and moment components were expressed through nondimensional aerodynamic coefficients that were dependent on perturbations of flight controls deflections: ailerons δ_A , elevator δ_E , rudder δ_R and motion parameters: longitudinal velocity u , sideslip angle $\beta = v/V_O$, angle of attack $\alpha = w/u$, roll rate p , pitch rate q and r yaw rate, where v and w stand for side and vertical velocity and V_O is the total velocity. The * symbol denotes nondimensional motion parameter, i.e. $p^* = pb/(2V)$, $q^* = q\bar{c}/(2V_O)$, $r^* = rb/(2V_O)$. Aerodynamic forces and moments were modeled according to [33]. The longitudinal force and vertical force dimensional coefficients for fixed configuration (no speed brakes and leading edge flaps deflections) and the aircraft at the trim (equilibrium) point is shown in Figs. 4 and 5.

The thrust force T was described as a first order spline with two intervals:

$$T = \begin{cases} T_{idle} + 0.02(T_{mil} - T_{idle})P_a & P_a < 50, \\ T_{mil} + 0.02(T_{max} - T_{mil})(P_a - 50) & P_a \geq 50, \end{cases} \quad (8)$$

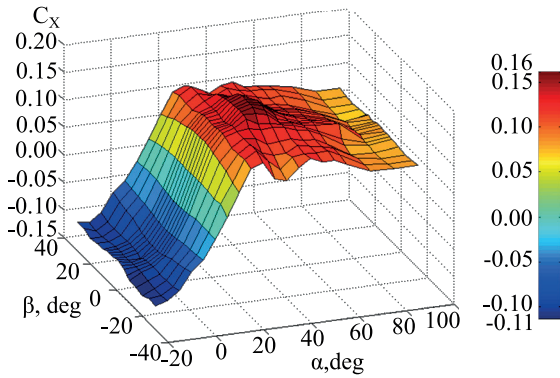


Fig. 4. Longitudinal force coefficient

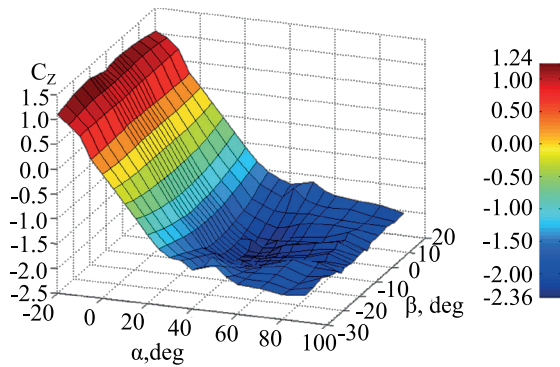


Fig. 5. Vertical force coefficient

where T_{idle} , T_{mit} and T_{max} are idle, military and maximum thrust force. The actual engine power level P_a was modelled as a first order lag with respect to commanded power level P_c :

$$\dot{P}_a = \frac{1}{\tau_{eng}} (P_c - P_a), \quad (9)$$

where commanded power level $P_c(\delta_{th})$ depends on the throttle setting δ_{th} and τ_{eng} is the engine time constant. Thrust force was modeled according to [33].

The equations of motion set was completed by including kinematic relationships between angular rates and attitude angles:

$$\begin{aligned} \dot{\phi} &= p + q \sin \phi \tan \theta + r \cos \phi \tan \theta, \\ \dot{\theta} &= q \cos \phi - r \sin \phi. \end{aligned} \quad (10)$$

Because the experiment lasted for a short period of time, fuel consumption was neglected and thus mass m was constant during the manoeuvre. It was also assumed that the flight control deflections do not influence inertia moments, so each I_{ij} (moment of inertia around j axis when object is rotated about i axis), was also constant. Engine angular rate was constant during the experiment leading to constant engine angular momentum H_T .

Atmosphere thermodynamic parameters were obtained from International Standard Atmosphere model [34] and the gravitational acceleration was obtained from the WGS-84 system

documentation [35].

As previously stated, the nonlinear model was excited with the sets of inputs described in Section 2 and its response was registered. From this point, the nonlinear model parameters (e.g. aerodynamic coefficients) were treated as unknown. On the basis of inputs and outputs of the nonlinear aircraft model a parameter estimation was performed. The system was identified as a linear model described by the equations presented in Subsection 3.2.

3.2. Linear model. The nonlinear equations of motion given in Eqs. (6) and (10) were linearized by using small perturbations theorem. This means that when a perturbation occurred each motion parameter was equal to its value in the equilibrium (0 subscript) and a small perturbation (denoted by Δ), e.g. $u = u_0 + \Delta u$.

In the equilibrium the aircraft was in steady straight symmetric flight. This implies that only $u_0 \neq 0$, $w_0 \neq 0$ and $\Theta_0 \neq 0$. Subtracting equations given for the trim point from the equations of the perturbed motion and neglecting small terms lead to the following:

$$\begin{aligned} \Delta X &= m(\Delta \dot{u} + \Delta q w_0), \\ \Delta Y &= m(\Delta \dot{v} + \Delta r u_0 - \Delta p w), \\ \Delta Z &= m(\Delta \dot{w} - \Delta q u_0), \\ \Delta L &= I_{xx} \Delta \dot{p} - I_{xz} \Delta \dot{r}, \\ \Delta M &= I_{yy} \Delta \dot{q}, \\ \Delta N &= I_{zz} \Delta \dot{r} - I_{xz} \Delta \dot{p}, \\ \Delta \dot{\phi} &= \Delta p + \Delta r \tan \theta, \\ \Delta \dot{\theta} &= \Delta q, \end{aligned} \quad (11)$$

where X , Y and Z are the longitudinal, lateral and vertical force, while L , M and N are rolling, pitching and yawing moment. Forces and moments were given by using first order Taylor series expansion around the trim point.

Forces and moment related to the longitudinal motion (X , Z , M) were dependent on flight parameters and control surfaces deflections that act in the aircraft vertical symmetry plane (u , w , q , δ_E):

$$\begin{aligned} \Delta X &= X_u \Delta u + X_w \Delta w + X_q \Delta q + X_{\delta_E} \Delta \delta_E, \\ \Delta Z &= Z_u \Delta u + Z_w \Delta w + Z_q \Delta q + Z_{\delta_E} \Delta \delta_E, \\ \Delta M &= M_u \Delta u + M_w \Delta w + M_q \Delta q + M_{\delta_E} \Delta \delta_E. \end{aligned} \quad (12)$$

Stability and control derivatives for ξ parameter were defined as:

$$\begin{aligned} X_\xi &= \frac{1}{m} \frac{\partial X}{\partial \xi}, \\ Z_\xi &= \frac{1}{m} \frac{\partial Z}{\partial \xi}, \\ M_\xi &= \frac{1}{I_{yy}} \frac{\partial M}{\partial \xi}. \end{aligned} \quad (13)$$

Similarly, force and moments related to lateral-directional motion (Y , L , N) were dependent only on the non-symmetrical flight parameters and controls (v , p , r , δ_A , δ_R):

$$\begin{aligned} \Delta Y &= Y_v \Delta v + Y_p \Delta p + Y_r \Delta r + Y_{\delta_A} \Delta \delta_A + Y_{\delta_R} \Delta \delta_R, \\ \Delta L &= L_v \Delta v + L_p \Delta p + L_r \Delta r + L_{\delta_A} \Delta \delta_A + L_{\delta_R} \Delta \delta_R, \\ \Delta N &= N_v \Delta v + N_p \Delta p + N_r \Delta r + N_{\delta_A} \Delta \delta_A + N_{\delta_R} \Delta \delta_R. \end{aligned} \quad (14)$$

Stability and control derivatives for ξ parameter were defined as:

$$\begin{aligned} Y_\xi &= \frac{1}{m} \frac{\partial Y}{\partial \xi}, \\ L_\xi &= \frac{I_{zz}}{I_{xx}I_{zz} - I_{xz}^2} \frac{\partial L}{\partial \xi} + \frac{I_{xz}}{I_{xx}I_{zz} - I_{xz}^2} \frac{\partial N}{\partial \xi}, \\ N_\xi &= \frac{I_{xz}}{I_{xx}I_{zz} - I_{xz}^2} \frac{\partial N}{\partial \xi} + \frac{I_{xx}}{I_{xx}I_{zz} - I_{xz}^2} \frac{\partial L}{\partial \xi}. \end{aligned} \quad (15)$$

The above definition for lateral-directional moments stability and control derivatives allowed to decouple rolling and yawing rates in (11).

Additionally, angle of attack perturbation $\Delta\alpha = \Delta w/u_0$ was used instead of vertical velocity perturbation Δw . Sideslip angle perturbation $\Delta\beta = \Delta v/V_0$ was used instead of side velocity perturbation Δv .

During the experiment the aircraft remained at almost the same altitude, thus the gravitational acceleration was constant and it was possible to decouple linearized equations of motion into longitudinal and lateral-directional sets:

$$\begin{aligned} \dot{\mathbf{x}}_{lon} &= \mathbf{A}_{lon} \mathbf{x}_{lon} + \mathbf{B}_{lon} \mathbf{u}_{lon}, \\ \dot{\mathbf{x}}_{lat} &= \mathbf{A}_{lat} \mathbf{x}_{lat} + \mathbf{B}_{lat} \mathbf{u}_{lat}. \end{aligned} \quad (16)$$

The state matrices were given as:

$$\begin{aligned} \mathbf{A}_{lon} &= \begin{bmatrix} X_u & X_\alpha - u_0 \alpha_0 & X_q & -g \cos \Theta_0 \\ Z_u & Z_\alpha & Z_q + 1 & -g \sin \Theta_0 / u_0 \\ M_u & M_\alpha & M_q & 0 \\ 0 & 0 & 1 & 0 \end{bmatrix}, \\ \mathbf{A}_{lat} &= \begin{bmatrix} Y_\beta & Y_p + \alpha_0 & Y_r - 1 & g \cos \Theta_0 / V_0 \\ L_\beta & L_p & L_r & 0 \\ N_\beta & N_p & N_r & 0 \\ 0 & 1 & \tan \Theta_0 & 0 \end{bmatrix} \end{aligned} \quad (17)$$

and the control matrices as:

$$\mathbf{B}_{lon} = \begin{bmatrix} X_{\delta_E} \\ Z_{\delta_E} \\ M_{\delta_E} \\ 0 \end{bmatrix}, \quad \mathbf{B}_{lat} = \begin{bmatrix} Y_{\delta_A} & Y_{\delta_R} \\ L_{\delta_A} & N_{\delta_R} \\ L_{\delta_A} & N_{\delta_R} \\ 0 & 0 \end{bmatrix}. \quad (18)$$

For the longitudinal motion the state and control vectors were $\mathbf{x}_{lon} = [\Delta u \quad \Delta \alpha \quad \Delta q \quad \Delta \theta]^T$ and $\mathbf{u}_{lon} = \Delta \delta_E$. In the case of

the lateral-directional motion, the corresponding vectors were

$$\mathbf{x}_{lat} = [\Delta \beta \quad \Delta p \quad \Delta r \quad \Delta \phi]^T \text{ and } \mathbf{u}_{lat} = [\Delta \delta_A \quad \Delta \delta_R]^T.$$

Linear model outputs were evaluated from:

$$\mathbf{y} = \mathbf{C}\mathbf{x} + \mathbf{D}\mathbf{u} + \mathbf{y}_0, \quad (19)$$

where state \mathbf{x} and control \mathbf{u} vectors consist of components related to longitudinal and lateral motion i.e. $\mathbf{x} = [x_{lon} \quad x_{lat}]^T$, $\mathbf{u} = [u_{lon} \quad u_{lat}]^T$, \mathbf{C} is the output matrix (identity matrix) and \mathbf{D} is the feedforward matrix (zero matrix).

4. Output error method

To perform the system identification a time domain output error method was used [3]. Therefore, the difference between registered outputs of the nonlinear aircraft model (measurements) \mathbf{z} and model outputs obtained from parameter estimation $\hat{\mathbf{y}}$ was to be minimized as shown in Fig. 6.

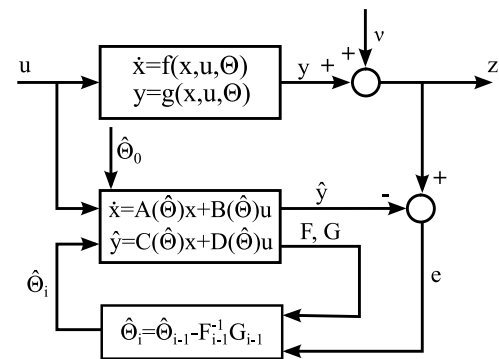


Fig. 6. Identification method scheme

This was achieved by applying the maximum likelihood principle i.e. finding a set of model parameters $\hat{\Theta}$ for which the probability p of observing measurements \mathbf{z} is maximized

$$\hat{\Theta} = \arg \{ \max_{\Theta} p(\mathbf{z} | \Theta) \}. \quad (20)$$

For multidimensional normal distribution the conditional probability can be expressed as:

$$p(\mathbf{z} | \Theta) = ((2\pi)^n |\mathbf{R}|)^{-N/2} \exp \left(-\frac{1}{2} \sum_{k=1}^N \mathbf{e}(t_k)^T \mathbf{R}^{-1} \mathbf{e}(t_k) \right), \quad (21)$$

where $\mathbf{e}(t_k) = \mathbf{z}(t_k) - \hat{\mathbf{y}}(t_k)$ is the output error at discrete time point t_k , n is the number of model outputs and \mathbf{R} is the noise covariance matrix and $|\mathbf{R}|$ denotes its determinant.

Due to the exponential function in Eq. (21) its maximization was replaced by negative log-likelihood minimization

$$\mathcal{L}(\Theta | \mathbf{z}) = -\ln p(\mathbf{z} | \Theta), \quad (22)$$

$$\mathcal{L}(\Theta | \mathbf{z}) = \frac{1}{2} \sum_{k=1}^N \mathbf{e}^T \mathbf{R}^{-1} \mathbf{e} + \frac{nN}{2} \ln(2\pi) + \frac{N}{2} \ln(|\mathbf{R}|). \quad (23)$$

The covariance matrix \mathbf{R} was estimated from

$$\hat{\mathbf{R}} = \frac{1}{N} \sum_{k=1}^N \mathbf{e}(t_k) \mathbf{e}(t_k)^T. \quad (24)$$

It is often assumed that the elements in output errors $\mathbf{e}(t_k)$ are independent (both, within the vector and in time) and only the diagonal elements of the covariance matrix \mathbf{R} are used. When this is assumed, substituting covariance matrix \mathbf{R} into Eq. (23) and neglecting constant terms allows to reduce cost function to:

$$J(\Theta) = |\mathbf{R}|. \quad (25)$$

The measurement noise covariance matrix \mathbf{R} is computed in each iteration.

For uncorrelated measurement errors the covariance matrix \mathbf{R} is diagonal, thus the cost function is:

$$J(\Theta) = \prod_{l=1}^n \frac{1}{N} \sum_{k=1}^N (z_l(t_k) - \hat{y}_l(t_k))^2. \quad (26)$$

Gauss-Newton algorithm was used to minimize the cost function. The parameters were updated according to the formula:

$$\hat{\Theta}_i = \hat{\Theta}_{i-1} + \mathbf{F}_{i-1}^{-1} \mathbf{G}_{i-1}. \quad (27)$$

The Fisher Information matrix \mathbf{F} was given as

$$\mathbf{F} = \sum_{k=1}^N \left[\frac{\partial \hat{\mathbf{y}}(t_k)}{\partial \Theta} \right]^T \mathbf{R}^{-1} \left[\frac{\partial \hat{\mathbf{y}}(t_k)}{\partial \Theta} \right]. \quad (28)$$

To evaluate gradients $\partial \hat{\mathbf{y}} / \partial \Theta$ central difference formula was used. Fisher Information matrix diagonal elements were used to determine relative standard deviations of the estimated parameters, i.e. $\sigma_{rel} = \sqrt{F_{ii}^{-1} / \hat{\Theta}_i}$. The gradient matrix \mathbf{G} was

$$\mathbf{G} = \sum_{k=1}^N \left[\frac{\partial \hat{\mathbf{y}}(t_k)}{\partial \Theta} \right]^T \mathbf{R}^{-1} \mathbf{e}(t_k). \quad (29)$$

5. Results

In the study, the output vector consists of all longitudinal and lateral motion states $\mathbf{y} = [x_{lon} \ x_{lat}]^T$. Stability and control derivatives were the estimated parameters and their initial values Θ_0 were obtained from previous studies [9]. For model structure determination, backward elimination method was used.

5.1. Noise-free. A noise free-case was investigated to evaluate the best possible accuracy of the system identification for experiments with multisine signals quantized at various levels. A nonlinear aircraft model described in Subsection 3.1 was excited with inputs shown in Section 2 and its response was registered. On the basis of this data, output error method presented in Section 4 was used to identify a linear system described in Subsection 3.2.

The time histories of the nonlinear model response and estimated outputs are shown in Figs. 7 and 8.

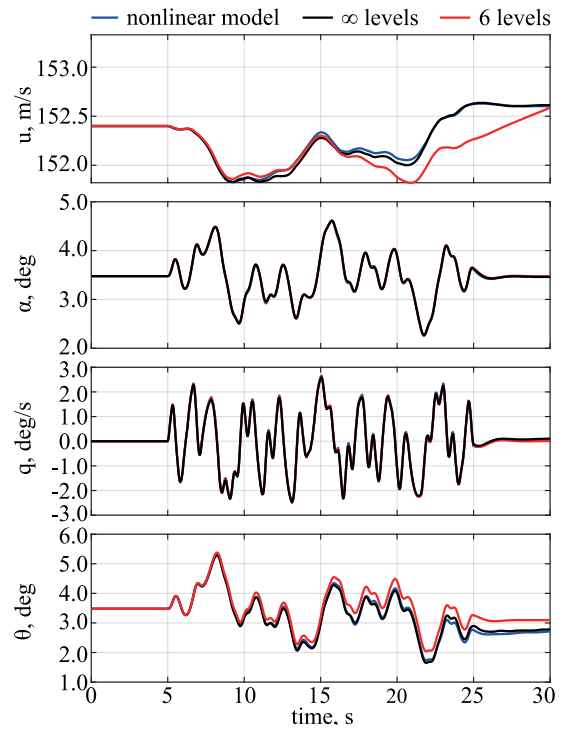


Fig. 7. Time histories – longitudinal motion variables

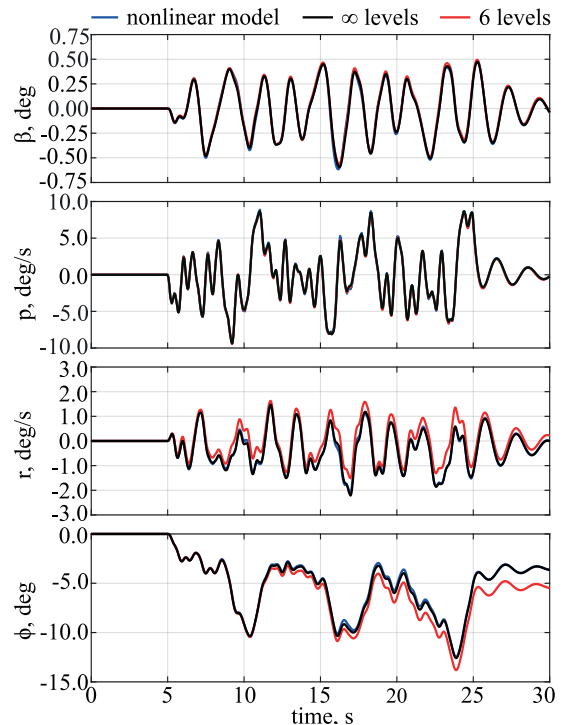


Fig. 8. Time histories – lateral motion variables

In Figs. 7 and 8 the blue lines represent the nonlinear model response, whereas black and red lines denote estimated model response. Black lines represent the linear model (obtained from

non-quantized multisines) response when excited with non-quantized multisines inputs. Red lines denote the linear model (obtained from multisine signals quantized at 6 levels) response when excited with quantized multisines inputs.

A very good visual match can be observed for the model estimated from non-quantized multisine inputs. This match drops with lower number of states that the input signal can accept. For the presented model, obtained from the quantized inputs, a good match can be observed for selected flight parameters. However, one must bear in mind that for the decoupled models all longitudinal or lateral-directional flight parameters must be considered jointly as the state variables influence one another.

Moreover, it can happen that a good visual match can be observed even when parameters were not accurately estimated e.g. due to overdetermined model structure. Thus, a common indicator of the system identification accuracy are the relative standard deviations σ_{rel} that express uncertainty of the estimates. A rule of thumb is that the relative standard deviation below 10% indicates accurate estimate [3]. The relative standard deviations of the identified stability and control derivatives when the multisine inputs were quantized at various levels are presented in Table 2. In Table 2 the ∞ symbol denotes the non-quantized inputs.

Table 2
Relative standard deviations – noise free

Θ	Quantization levels								
	∞	16	14	12	10	8	6	4	2
X_u	0.85	0.87	0.89	0.96	0.90	0.83	0.86	0.77	2.04
X_α	8.60	9.87	9.76	9.47	9.27	8.05	19.21	20.17	19.02
X_q	9.56	7.41	7.20	7.83	8.12	9.37	12.39	21.64	31.67
X_{δ_E}	6.63	8.29	8.08	8.70	8.21	9.48	13.95	17.06	18.18
Z_α	0.22	0.29	0.28	0.25	0.29	0.29	0.38	0.47	1.15
Z_q	0.13	0.17	0.16	0.15	0.17	0.17	0.19	0.22	0.45
M_α	0.10	0.14	0.14	0.12	0.14	0.14	0.17	0.20	0.42
M_q	0.20	0.27	0.26	0.24	0.27	0.27	0.31	0.35	0.67
M_{δ_E}	0.08	0.12	0.11	0.10	0.12	0.12	0.15	0.17	0.37
Y_β	5.98	6.97	7.64	7.57	8.35	8.32	8.90	11.34	28.76
Y_p	3.16	4.22	4.23	4.12	4.49	4.48	4.74	5.37	7.73
Y_r	0.83	1.15	1.14	1.12	1.24	1.23	1.32	1.55	2.88
L_β	0.32	0.34	0.34	0.34	0.35	0.35	0.37	0.40	0.77
L_p	0.24	0.26	0.26	0.25	0.26	0.27	0.28	0.30	0.54
L_r	8.07	8.44	8.20	8.16	8.48	8.70	9.04	10.54	38.44
L_{δ_A}	0.15	0.16	0.16	0.15	0.16	0.16	0.17	0.19	0.41
L_{δ_R}	0.75	0.78	0.77	0.76	0.79	0.80	0.83	0.92	2.07
N_β	0.95	1.33	1.32	1.30	1.44	1.43	1.54	1.83	3.82
N_p	4.49	5.76	5.84	5.65	6.13	6.04	6.37	6.95	8.17
N_r	5.19	7.29	7.35	7.15	8.01	7.83	8.42	9.38	14.06
N_{δ_A}	4.05	5.42	5.45	5.28	5.76	5.74	6.02	6.77	8.54
N_{δ_R}	0.85	1.19	1.18	1.16	1.29	1.28	1.38	1.62	3.20

From Table 2 it can be seen that the inputs quantized at 8 or more levels allow to obtain accurate estimates. The inaccurate

estimates were observed first in the longitudinal motion parameters. The inaccuracies in lateral-directional stability and control derivatives started to occur when the multisine inputs were quantized at 4 levels. Generally, it can be said that the relative standard deviations increase when the signals are quantized with fewer levels. Due to the complex relation between system parameters, it may happen that for a lower quantization level a particular estimate is more accurate than when signal is quantized at lower level. However, this will be reflected in increased relative standard deviations of other estimated parameters.

For validation, a set of inputs that was not used in the identification was selected. The nonlinear model was excited with multi-step inputs. This could allow to find unmodelled dynamics in the estimated models, as e.g. the multi-step signals have continuous power spectrum and multisines have discrete spectrum. Conventional multi-step inputs were used for that purpose: 3211 elevator input, 121 ailerons deflection and rudder doublet. According to [36], *RMS* can be used to assess the accuracy for the data not used in parameter estimation and for fixed-wing aircraft $RMS < 1.0$ denote accurate results. The *RMS* is presented in Table 3. It can be seen that this supports previous conclusions. The *RMS* increases when inputs are quantized with less levels. For elevator input the model was accurate when signals were quantized at least at 8 levels and for ailerons or rudder input it was accurate for at least 6 quantization levels.

Table 3
Model verification (RMS) – noise free

	Quantization levels								
	∞	16	14	12	10	8	6	4	2
Ailerons	0.31	0.32	0.32	0.33	0.349	0.39	0.56	1.04	1.45
Elevator	0.38	0.39	0.40	0.42	0.55	0.72	1.062	1.41	1.87
Rudder	0.29	0.32	0.34	0.36	0.40	0.45	0.69	1.06	1.41

The validation was also done by using Theil inequality coefficient (*TIC*) that presents estimated model predicting capabilities. According to [36], $TIC < 0.3$ denotes good forecast for fixed wing aircraft. To evaluate *TIC* the same inputs were used as for *RMS*, and the results are presented in Table 4. It can be seen that predicting capabilities are good for the models estimated with high accuracy. The predicting capabilities drop for models estimated when inputs with less quantization levels were used. In longitudinal motion, the forecasts would be good for the models obtained with multisines with at least 8 possible states. In lateral-directional motion, models obtained with at least 6 quantization levels provide good prediction.

Table 4
Model verification (TIC) – noise free

	Quantization levels								
	∞	16	14	12	10	8	6	4	2
Ailerons	0.06	0.06	0.07	0.09	0.13	0.18	0.21	0.31	0.39
Elevator	0.10	0.10	0.12	0.16	0.21	0.24	0.31	0.48	0.62
Rudder	0.06	0.06	0.07	0.09	0.14	0.19	0.22	0.31	0.38

5.2. Identification from frequency responses. The system was identified from frequency responses to verify the results obtained with output error method time domain approach. It was already shown in [15, 28] that this method provides accurate estimates when the system is excited with multisine inputs. The CIFER software [36] was used for that purpose.

The input autospectrum \hat{S}_{xx} , output autospectrum \hat{S}_{yy} and cross spectrum \hat{S}_{xy} for a Single-Input/Single-Output system were evaluated from:

$$\begin{aligned}\hat{S}_{xx}(f) &= \frac{1}{Un_r} \sum_{k=1}^{n_r} \frac{2}{T} |X(f)|^2, \\ \hat{S}_{yy}(f) &= \frac{1}{Un_r} \sum_{k=1}^{n_r} \frac{2}{T} |Y(f)|^2, \\ \hat{S}_{xy}(f) &= \frac{1}{Un_r} \sum_{k=1}^{n_r} \frac{2}{T} |X^\dagger(f)Y(f)|,\end{aligned}\quad (30)$$

where $X(f)$ and $Y(f)$ are input and output Fourier transforms, n_r is the number of time segments, U is the correction factor and \dagger symbol denotes complex conjugate. The half sine-windows were used to reduce spectral leakage, thus $U = 0.707$.

The frequency response function $H(f)$ was evaluated from the Single-Input/Single-Output system spectra estimates:

$$\hat{H}(f) = \frac{\hat{S}_{xy}(f)}{\hat{S}_{xx}(f)}.\quad (31)$$

On the basis of the Single-Input/Single-Output solution, frequency responses for the Multiple-Input/Single-Output system estimates were found:

$$\hat{\mathbf{H}}(f) = \hat{\mathbf{S}}_{xx}^{-1}(f) \hat{\mathbf{S}}_{xy}(f),\quad (32)$$

where $\hat{\mathbf{S}}_{xx}$ is the matrix of estimated auto-spectra between the inputs and outputs and $\hat{\mathbf{S}}_{xy}$ is the estimated cross-spectra matrix between each input and single output. Multiple-Input/Multiple-Output solution was obtained by gathering the Multiple-Input/Single-Output results.

The frequency responses were obtained for various windows length and then conditioned to obtain accurate results in the whole bandwidth.

Stability and control derivatives of the linear model were found by minimizing the cost function:

$$\begin{aligned}J &= \sum_{k=1}^{n_r} \left(\frac{20}{n_\omega} \sum_{\omega} W_\gamma (W_m (|T_m| - |\hat{T}_m|)^2 \right. \\ &\quad \left. + W_p (\angle T_m - \angle \hat{T}_m)^2 \right),\end{aligned}\quad (33)$$

where T_m and \hat{T}_m are transfer functions, $(1, \dots, n_r)$, obtained from the data (nonlinear model) and for the estimated linear model. Each function was fitted for frequencies ω , $(1, \dots, n_\omega)$, at which sufficient amount of information for modelling was

present, i.e. magnitude squared coherence $\hat{\gamma}_{xy}^2 > 0.6$ [36]:

$$\hat{\gamma}_{xy}^2(f) = \frac{|\hat{S}_{xy}(f)|^2}{|\hat{S}_{xx}(f)| |\hat{S}_{yy}(f)|}.\quad (34)$$

The magnitude and phase weights were $W_m = 1.0$ and $W_p = 0.01745$, respectively. The coherence weighting W_γ was set to emphasize the most reliable data:

$$W_\gamma = \left[1.58(1 - e^{-\gamma_{xy}^2}) \right]^2.\quad (35)$$

Stability and control derivatives were estimated from frequency responses by using the same data set and linear model equations as in the noise-free case. Their relative standard deviations for manoeuvres with multisine excitations with various quantization levels are shown in Table 5.

Table 5
Relative standard deviations – frequency responses identification

Θ	Quantization levels								
	∞	16	14	12	10	8	6	4	2
X_u	0.84	0.87	0.80	0.95	0.93	0.80	0.84	0.80	2.14
X_α	8.69	9.73	9.97	9.22	8.59	7.70	18.67	20.91	18.63
X_q	9.47	6.84	6.51	7.97	8.33	8.70	11.54	21.30	31.36
X_{δ_E}	6.41	7.51	7.93	8.99	8.46	9.60	14.01	15.53	17.20
Z_α	0.20	0.27	0.27	0.23	0.30	0.29	0.36	0.49	1.08
Z_q	0.13	0.16	0.15	0.15	0.16	0.18	0.18	0.23	0.42
M_α	0.10	0.13	0.15	0.12	0.14	0.14	0.16	0.21	0.39
M_q	0.19	0.25	0.26	0.23	0.27	0.27	0.31	0.34	0.64
M_{δ_E}	0.08	0.12	0.11	0.09	0.12	0.13	0.14	0.18	0.36
Y_β	5.67	6.66	7.99	7.40	8.25	8.25	9.30	11.53	27.79
Y_p	3.22	3.80	4.30	4.22	4.16	4.16	4.86	5.53	7.93
Y_r	0.85	1.07	1.12	1.08	1.27	1.22	1.29	1.56	2.91
L_β	0.33	0.32	0.35	0.35	0.32	0.37	0.36	0.42	0.77
L_p	0.25	0.24	0.25	0.23	0.26	0.27	0.25	0.28	0.49
L_r	8.26	8.32	7.60	8.42	8.34	8.90	9.45	10.71	38.20
L_{δ_A}	0.16	0.16	0.15	0.15	0.15	0.14	0.16	0.18	0.38
L_{δ_R}	0.77	0.72	0.69	0.77	0.72	0.72	0.87	0.93	1.92
N_β	0.90	1.30	1.19	1.35	1.35	1.37	1.47	1.66	3.60
N_p	4.59	5.52	5.98	5.88	6.30	5.46	6.12	6.75	8.19
N_r	5.27	7.38	6.73	7.04	7.93	7.99	7.72	8.99	13.59
N_{δ_A}	4.01	5.13	4.97	5.15	5.28	5.42	5.54	6.88	8.07
N_{δ_R}	0.83	1.18	1.20	1.10	1.27	1.16	1.26	1.48	3.16

It can be seen that the outcomes are in good agreement with the results obtained when output error method was used. The accuracy of the estimated stability and control derivatives drops for models identified with multisine inputs with less quantization levels. Similarly to the output error outcomes, in the longitudinal motion the estimates are acceptable for multisines quantized at 8 or more levels. In lateral-directional motion accurate results were obtained when inputs were quantized at 6 or more levels. It can be observed that generally, identification from frequency responses allowed to obtain slightly better results. This

is because in the presented frequency domain approach greater emphasis was put on more accurate data. In the output error method all data points were equally weighted.

5.3. Noise in the outputs. In order to investigate how the measurement noise affects the identification for quantized inputs, a white noise with 5% noise to signal ratio was added to the outputs after the nonlinear model response was generated. The rest of the procedure was the same as for parameter estimation in the noise free-case. The outcomes are presented in Table 6.

Table 6
Relative standard deviations – noise in the outputs

Θ	Quantization levels								
	∞	16	14	12	10	8	6	4	2
X_u	1.19	1.65	1.89	1.59	2.13	4.83	4.80	4.73	5.94
X_α	8.84	8.81	8.79	9.13	9.73	15.87	19.68	19.46	20.29
X_q	9.08	9.98	9.08	8.78	9.04	17.71	17.21	26.88	27.92
X_{δ_E}	6.28	8.22	8.03	9.83	9.34	18.96	15.78	14.16	22.90
Z_α	0.56	0.91	2.28	2.31	2.34	2.33	2.32	2.41	2.82
Z_q	0.33	0.93	1.16	1.38	1.19	1.40	1.44	1.46	1.59
M_α	0.27	0.46	1.14	1.16	1.16	1.16	1.19	1.20	1.26
M_q	0.55	1.20	1.26	2.40	2.31	2.44	2.53	2.53	2.58
M_{δ_E}	0.21	0.93	0.11	0.90	0.13	0.91	0.93	0.93	1.01
Y_β	6.40	7.10	7.64	7.63	7.84	9.77	10.06	12.25	30.01
Y_p	3.34	3.10	4.24	4.44	4.22	6.74	6.97	7.06	8.17
Y_r	0.87	0.89	1.14	1.67	1.61	1.76	1.83	1.94	3.06
L_β	0.55	2.15	2.34	2.05	2.37	2.07	2.10	2.07	2.23
L_p	0.44	0.41	0.46	1.51	1.28	1.52	1.53	1.53	1.54
L_r	8.67	8.80	8.05	9.06	9.65	18.81	20.91	24.73	36.84
L_{δ_A}	0.32	0.75	1.16	1.33	0.18	1.35	1.37	1.36	1.34
L_{δ_R}	1.63	1.89	1.77	3.72	4.47	4.51	4.51	4.98	5.70
N_β	0.99	1.06	1.32	1.85	1.36	1.96	2.05	2.21	3.92
N_p	4.71	5.69	5.86	7.99	8.73	9.15	9.36	9.14	9.07
N_r	5.27	7.12	7.36	8.47	9.48	10.18	10.66	11.42	15.73
N_{δ_A}	4.17	4.87	5.45	7.43	7.41	7.83	8.08	8.19	9.08
N_{δ_R}	0.91	1.04	1.18	1.80	1.92	1.93	2.01	2.11	3.55

It can be seen that the noise lowered the accuracy of the estimated parameters regardless of the quantization level. When noise was present in the outputs the estimates were considered not accurate enough when the quantization level was 8. In this case it was related to both – longitudinal and lateral directional motion.

The estimated models responses were analyzed for data that was not used in parameter estimation. The same inputs were used as in the noise-free case. *RMS* for models obtained with various inputs quantization levels is shown in Table 7. It can be seen that the *RMS* confirms previous conclusions. The accuracy is lower than for the noise-free case and it drops when signals are quantized with less levels as can be expected. When noise was present in the outputs the results were found accurate for

Table 7
Model verification (*RMS*) – noise in the outputs

	Quantization levels								
	∞	16	14	12	10	8	6	4	2
Ailerons	0.32	0.33	0.35	0.45	0.62	1.05	1.16	1.31	1.59
Elevator	0.40	0.42	0.47	0.50	0.68	1.13	1.34	1.54	2.01
Rudder	0.31	0.33	0.35	0.48	0.75	1.06	1.25	1.48	1.63

models obtained with multisines quantized with more than 8 states.

The *TIC* for the models validated with inputs not used in system identification is shown in Table 8. Similar conclusions can be made as for the *RMS* – predicting capabilities are lower than for the noise-free case and they decreased when estimates were obtained for inputs with fewer quantization levels. For both, longitudinal and lateral motion, multisines with more than 8 states allow for good forecasting.

Table 8
Model verification (*TIC*) – noise in the outputs

	Quantization levels								
	∞	16	14	12	10	8	6	4	2
Ailerons	0.08	0.09	0.12	0.16	0.22	0.30	0.35	0.41	0.51
Elevator	0.11	0.11	0.13	0.16	0.24	0.31	0.37	0.52	0.64
Rudder	0.06	0.09	0.12	0.17	0.23	0.30	0.31	0.33	0.40

The presented output-error equations are valid under white noise measurement assumption. Thus, including coloured noise would be introducing modelling error. The aim of the paper was to assess quantized multisine inputs and not to check the output-error sensitivity to noise type. Therefore, only white noise was present in the data.

5.4. Noise in the inputs. The same process was performed when measurement noise was available in the input data only. The outcomes of the parameter estimation are presented in Table 9.

Similarly to the case when noise was present in the outputs, the accuracy of the estimates was lowered. The input provided the object response that did not contain sufficient amount of information when multisines were quantized with 8 discrete states for longitudinal and 10 for lateral-directional motion. This happened because the system identification algorithm was unable to distinguish between the noise and high frequency components that should be present in the input. Noise presence in the inputs lead to increased error in all estimates as can be seen when comparing average relative standard deviation for all estimates presented in Fig. 9.

The *RMS* for the models validated with inputs not used in system identification is shown in Table 10. Again, it can be seen that the accuracy drops when fewer levels are used for quantization. However, this time it is possible to observe that the *RMS* is above the threshold for ailerons and elevator when 8 levels are used and for 10 levels for rudder deflection. Lower *RMS*

Table 9
Relative standard deviations – noise in the inputs

Θ	Quantization levels								
	∞	16	14	12	10	8	6	4	2
X_u	1.56	1.59	1.59	2.33	3.02	6.12	10.96	9.57	5.24
X_α	9.18	9.27	9.42	9.65	9.81	18.57	18.17	21.26	37.46
X_q	8.32	8.36	9.19	8.9	9.32	17.48	17.49	22.15	25.12
X_{δ_E}	8.41	8.7	8.67	9.3	9.86	18.81	20.19	25.23	41.77
Z_α	0.52	1.07	2.47	2.48	2.5	2.49	2.46	2.49	3.03
Z_q	0.33	0.76	1.03	1.26	1.28	1.27	1.26	1.28	1.51
M_α	0.28	0.41	1.03	1.21	1.21	1.23	1.2	1.22	1.49
M_q	0.53	0.87	1.05	2.36	2.4	2.38	2.38	2.43	2.87
M_{δ_E}	0.12	1.11	0.2	1.11	0.23	1.13	1.13	1.17	1.44
Y_β	6.78	7.99	8.45	8.59	10.37	10.34	10.93	16.39	31.74
Y_p	4.05	5.23	4.85	5.3	5.5	5.49	5.76	6.39	8.78
Y_r	0.89	1.16	1.18	1.17	1.29	1.34	1.38	1.65	3.12
L_β	0.61	2.37	2.37	2.36	2.36	2.38	2.37	2.41	2.79
L_p	0.44	0.47	0.45	1.26	1.27	1.28	1.3	1.31	1.53
L_r	8.25	9.09	9.57	9.76	10.06	17.33	20.69	21.43	37.38
L_{δ_A}	0.36	0.67	1.02	1.16	1.17	1.17	1.18	1.2	1.45
L_{δ_R}	1.73	1.79	2.16	3.77	3.8	3.82	3.85	4.94	6.05
N_β	0.92	1.34	1.98	2.38	2.57	2.57	3.55	3.85	6.83
N_p	4.53	5.65	5.81	6.54	7.02	6.94	8.27	8.84	9.15
N_r	5.97	7.21	8.14	8.08	9.94	10.76	11.34	12.29	16.99
N_{δ_A}	4.88	5.39	6.03	6.26	6.73	7.71	8.01	8.75	9.6
N_{δ_R}	0.83	1.2	1.79	2.24	2.35	2.37	2.46	2.77	4.21

Table 10
Model verification (RMS) – noise inputs

	Quantization levels								
	∞	16	14	12	10	8	6	4	2
Ailerons	0.33	0.33	0.36	0.46	0.68	1.12	1.25	1.47	1.73
Elevator	0.42	0.44	0.49	0.48	0.71	1.07	1.41	1.69	2.20
Rudder	0.31	0.34	0.36	0.59	1.02	1.25	1.46	1.65	1.79

Table 11
Model verification (TIC) – noise inputs

	Quantization levels								
	∞	16	14	12	10	8	6	4	2
Ailerons	0.09	0.09	0.12	0.16	0.22	0.31	0.38	0.45	0.56
Elevator	0.12	0.13	0.14	0.18	0.24	0.32	0.38	0.54	0.66
Rudder	0.06	0.10	0.12	0.18	0.31	0.32	0.34	0.36	0.46

were used for quantization. For ailerons and elevator this was true for 8 quantization states.

Again, only white noise was present in the data.

6. Conclusions

In this paper an experiment with simultaneous multisine ailerons, elevator and rudder excitations was presented. The inputs were quantized at various levels and used to excite a non-linear aircraft model. The response of the object was registered and used to estimate a linear model by using time domain output error method.

It was shown that the linear model provided representative aircraft response. When measurement noise was not in the data, quantized inputs allowed to obtain accurate stability and control derivatives from system identification when the the inputs were quantized at 8 levels or more. Results with slightly higher accuracy were obtained when identification was performed from frequency responses.

When noise was present in the outputs, the accuracy was lowered and more quantization levels were required to obtain accurate estimates. This was even more visible when measurement noise was present in the inputs.

In future steps, quantized inputs should be applied on a real aircraft during flight campaign. Moreover, it should be investigated how the values of the quantized steps and the switching times selection influence the accuracy of the system identification results.

REFERENCES

- [1] Certification Specifications for Aeroplane Flight Simulation Training Device, European Space Agency, Technical Report CS-FSTD(A), Paris, 2018.
- [2] FAA Approval of Aviation Training Devices and Their Use for Training and Experience, Federal Aviation Administration, Technical Report 61-136B, Washington D.C., 2018.

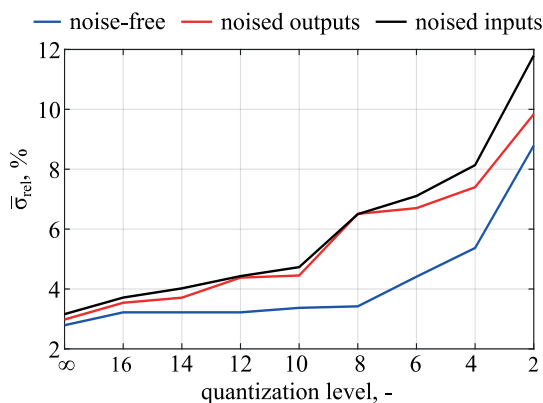


Fig. 9. Average relative standard deviation

for the rudder validation input can be explained by Y_β and L_r relative standard deviations that dropped below 10% when inputs were quantized at 10 levels (observing those parameters is related mostly to rudder deflection).

The TIC for the models validated with inputs not used in system identification is shown in Table 11. Again, lower forecasting capabilities can be observed for models estimated for inputs with less states. It can be seen that predicting capabilities for the rudder were good enough when more than 10 levels

- [3] R.V. Jategaonkar, “Flight Vehicle System Identification: A Time Domain Methodology”, *Progress in Astronautics and Aeronautics*, AIAA, Reston, VA, 2015, doi: 10.2514/4.102790.
- [4] J.A. Grauer, “Real-Time Data-Compatibility Analysis Using Output Error Parameter Estimation”, *J. Aircr.* 52(3), 940–947 (2015), doi: 10.2514/1.C033182.
- [5] C. Deiler, “Aerodynamic Modeling, System Identification, and Analysis of Iced Aircraft Configurations”, *J. Aircr.* 55(1), 145–161 (2017), doi: 10.2514/1.C034390.
- [6] E. Özger, “Parameter Estimation of Highly Unstable Aircraft Assuming Linear Errors”, *AIAA Atmospheric Flight Mechanics Conference*, Minneapolis, 2012, doi: 10.2514/6.2012-4511.
- [7] B. Mettler, T. Kanade, and M.B. Tischler, “System identification modeling of a model-scale helicopter”, Technical Report CMURI-TR-00-03, Robotics Institute, Pittsburgh, 2000.
- [8] L. Baranowski, B. Gadowski, P. Majewski, and J. Szymonik, “35 mm ammunition’s trajectory model identification based on firing tables”, *Bull. Pol. Ac.: Tech.* 66(5), 635–643 (2018), doi: 10.24425/bpas.2018.124279.
- [9] P. Lichota, M. Jacewicz, and J. Szulczyk, “Spinning gasodynamic projectile system identification experiment design”, *Aircr. Eng. Aerosp. Technol.* 92(3), 452–459 (2020), doi: 10.1108/AEAT-06-2019-0124.
- [10] M. Jirgl, L. Obsilova, J. Boril, and R. Jalovecky, “Parameter identification for pilot behaviour model using the MATLAB system identification toolbox”, *2017 International Conference on Military Technologies (ICMT)*, Brno, 2017, doi: 10.1109/MILTECHS.2017.7988824.
- [11] A. Kopyt and M. Žugaj, “Analysis of Pilot Interaction with the Control Adapting System for UAV”, *J. Aerosp. Eng.* 33(4), 1–7 (2020), doi: 10.1061/(ASCE)AS.1943-5525.0001109.
- [12] P. Lichota, K. Sibilski, and P. Ohme, “D-Optimal Simultaneous Multistep Excitations for Aircraft Parameter Estimation”, *J. Aircr.* 54(2), 747–758 (2017), doi: 0.2514/1.C033794.
- [13] M.S. Roeser and N. Fezans, “Method for Designing Multi-Input System Identification Signals Using a Compact Time-Frequency Representation”, *CEAS Aeronaut. J.*, (in press).
- [14] E.A. Morelli, “Multiple Input Design for Real-Time Parameter Estimation in the Frequency Domain”, *13th IFAC Conference on System Identification*, IFAC Paper REG-360, Rotterdam, 2003.
- [15] M.B. Tischler, C.M. Ivler, and T. Berger, “Comment on Method for Real-Time Frequency Response and Uncertainty Estimation”, *J. Guid. Control Dyn.* 38(3), 547–549 (2015), doi: 10.2514/1.G000780.
- [16] B. Martos and A. Noriega, “A Method for Real-Time Pilot Modeling and Multisine Tracking Input Design”, *AIAA Scitech 2019 Forum*, AIAA 2019–1318, San Diego, 2019, doi: 10.2514/6.2019-1318.
- [17] J.A. Grauer, E.A. Morelli, and D.G. Murri, “Flight-Test Techniques for Quantifying Pitch Rate and Angle-of-Attack Rate Dependencies”, *J. Aircr.* 54(6), (2017), doi: 10.2514/1.C034407.
- [18] M.J. Schmitz and R.A. Green, “Multisine excitation design to increase the efficiency of system identification analysis through undersampling and DFT”, *Measurement* 45(6), 1576–1586 (2013), doi: 10.1016/j.measurement.2012.02.019.
- [19] E. Keikha, A. Al Mamun, T.H. Lee, and C.S. Bhatia, “Multi-frequency Technique for Frequency Response Measurement and its Application to Servo System with Friction”, *IFAC Proc. Volumes* 44(1), 5273–5278 (2011), doi: 10.3182/20110828-6-IT-1002.02670.
- [20] E. Geerardyn, Y. Rolain, and J. Schoukens, “Design of Quasilogarithmic Multisine Excitations for Robust Broad Frequency Band Measurements”, *IEEE Trans. Instrum. Meas.* 62(5), 1364–1372 (2013), doi: 10.1109/TIM.2012.2232474.
- [21] P. Lichota, J. Szulczyk, D.A. Noreña, F.A. Vallejo Monsalve, “Power spectrum optimization in the design of multisine manoeuvre for identification purposes”, *J. Theor. Appl. Mech.* 54(4), 1193–1203 (2017), doi: 10.15632/jtam-pl.55.4.1193.
- [22] M. Alabsi and T. Fields, “Quadrotor aircraft intelligent system identification experiment design”, *Proc. Inst. Mech. Eng. Part G–J. Aerosp. Eng.* 233(13), 4911–4925 (2019), doi: 10.1177/0954410019833209.
- [23] M. Schroeder, “Synthesis of low-peak-factor signals and binary sequences with low autocorrelation”, *IEEE Trans. Inf. Theory* 16(1), 85–89 (1970), doi: 10.1109/TIT.1970.1054411.
- [24] J. Ojarand and M. Min, “Recent Advances in Crest Factor Minimization of Multisine” *Elektronika i Elektrotehnika* 23(2), 59–62 (2017), doi: 10.5755/j01.eie.23.2.18001.
- [25] Y. Yang, F. Zhang, K. Tao, B. Sanchez, H. Wen, and Z. Teng, “An improved crest factor minimization algorithm to synthesize multisines with arbitrary spectrum”, *Physiol. Meas.* 36(5), 895–910 (2015), doi: 10.1088/0967-3334/36/5/895.
- [26] M.J. Schmitz and R.A. Green, “Multisine Excitation Design Using Synchronous Square Wave Sources”, *2013 IEEE International Instrumentation and Measurement Technology Conference*, Minneapolis, 2013, pp. 319–322, doi: 10.1109/I2MTC.2013.6555432.
- [27] P. Young and R.J. Patton, “Comparison of Test Signals for Aircraft Frequency Domain Identification”, *J. Guid. Control Dyn.* 13(3), 430–438 (1990), doi: 10.2514/3.25355.
- [28] P. Lichota, J. Szulczyk, M.B. Tischler, and T. Berger, “Frequency Responses Identification from Multi-Axis Maneuver with Simultaneous Multisine Inputs” *J. Guid. Control Dyn.* 42(11), 2550–2556 (2019), doi: 10.2514/1.G004346.
- [29] O. Mårtens and M. Min, “Multifrequency Bio-Impedance Measurement: Undersampling Approach”, *Proceedings of the 6th Nordic Signal Processing Symposium NORSIG 2004*, Espoo, Finland, 2004, pp. 145–148.
- [30] C. Deiler and N. Fezans, “VIRTAC—A Family of Virtual Test Aircraft for Use in Flight Mechanics and GNC Benchmarks”, *AIAA Scitech 2019 Forum*, AIAA 2019–0950, San Diego, 2019, doi: 10.2514/6.2019-0950.
- [31] S. Topczewski, P. Bibik, and M. Zugaj, “Development of an automatic system for helicopter approach to a moving vessel”, *44th European Rotorcraft Forum 2018, Delft, 2018*, pp. 1425–1430.
- [32] S. Topczewski, J. Narkiewicz, and P. Bibik, “Helicopter Control During Landing on a Moving Confined Platform”, *IEEE Access* 8, 107315–107325 (2020), doi: 0.1109/ACCESS.2020.3000294.
- [33] L.T. Nguyen, M.E. Ogburn, W.P. Gilbert, K.S. Kibler, P.W. Brown, and P.L. Deal, “Simulator Study of Stall/Post-Stall Characteristics of a Fighter Airplane with Relaxed Longitudinal Static Stability”, NASA, Technical Report TP-1538, Hampton, 1979.
- [34] “U.S. Standard Atmosphere”, National Oceanic and Atmospheric Administration, Technical Report NOAA-S/T-76–1562, Washington D.C, 1976.
- [35] “Department of Defense World Geodetic System 1984, Its Definition and Relationships With Local Geodetic Systems”, National Imagery and Mapping Agency, Washington D.C, Technical Report TR8350.2, 1984.
- [36] M.B. Tischler and R.K. Rempke, “Aircraft and Rotorcraft System Identification”, *AIAA Education Series*, AIAA, Reston, VA, 2012, doi: 10.2514/4.868207.